Chemical Engineering Science 65 (2010) 2472–2480

Contents lists available at ScienceDirect

Chemical Engineering Science

journal homepage: www.elsevier.com/locate/ces

Reactor simulation of benzene ethylation and ethane dehydrogenation catalyzed by ZSM-5: A multiscale approach

N. Hansen [a,*], R. Krishna [b], J.M. van Baten [b], A.T. Bell [c,*], F.J. Keil [a]

[a] Department of Chemical Engineering, Hamburg University of Technology, D-21073 Hamburg, Germany
[b] Van't Hoff Institute for Molecular Sciences, University of Amsterdam, 1018 WV Amsterdam, The Netherlands
[c] Department of Chemical Engineering, University of California, Berkeley, CA 94720-1462, USA

ARTICLE INFO

Article history:
Received 7 July 2009
Received in revised form
3 December 2009
Accepted 21 December 2009
Available online 4 January 2010

Keywords:
Zeolites
Mixture diffusion
Molecular simulations
Heterogeneous catalysis
Alkylation
Dehydrogenation

ABSTRACT

Rate expressions are vital for analysis, design and operation of chemical reactors. However, due to a simplified picture of the underlying physical processes, empirical power-law (PL) fits, and Langmuir–Hinshelwood (LH) expressions may not be reliable when extrapolated to conditions which were not included in the parameterization process. In the present work the extrapolation ability of LH and PL models are evaluated for the zeolite catalyzed alkylation of benzene with ethene. For this purpose, extrapolated data are compared to results obtained from a detailed continuum model based on a multiscale approach (Hansen et al., J. Phys. Chem. C, 113 (2009) 235–246). It is demonstrated that extrapolation is in particular questionable if the gas phase composition is outside the fitting range. A second purpose of the present work is the extension of our continuum model to include the dehydrogenation of ethane. The parameters describing adsorption and diffusion are obtained from Monte Carlo and molecular dynamics simulations, respectively. Reaction rate constants are derived from quantum chemical calculations and transition state theory. We have used the extended continuum model in the design equation of a fixed bed reactor and simulated the dehydroalkylation activity for different input conditions. Furthermore, the benefit from removing hydrogen from the reaction mixture using a membrane reactor is discussed.

1. Introduction

Gas phase alkylation of benzene using zeolite catalysts is an environmentally friendly alternative to liquid phase processes which deal with problems of corrosion and waste disposal (Weitkamp and Puppe, 1999; Perego and Ingallina, 2002). The zeolite ZSM-5 has been used for catalyzing the gas phase ethylation in the Mobil/Badger process since 1980 (Dwyer et al., 1976; Haag et al., 1984; Weitkamp, 1985). We have shown recently that the apparent kinetics of this process can be successfully predicted by combining atomistic and continuum modeling (Hansen et al., 2008, 2009). A major advantage of this multiscale approach is that it strictly separates intrinsic kinetics from adsorption and transport phenomena and thus discriminates between scale-dependent and scale-independent processes. By contrast, we note that the kinetic models used in industrial practice are frequently power law (PL) or Langmuir–Hinshelwood (LH) type expressions (Mezaki and Inoue, 1991; Bos et al., 1997; Berger et al., 2001). Depending on the data used in identifying the parameters in these models, such models may include internal transport effects or even external and internal transport effects, in addition to intrinsic reaction kinetics. Moreover, for mixtures containing molecules with different saturation loadings the LH approach has been shown to be thermodynamically inconsistent (Krishna and Baur, 2005; Baur and Krishna, 2005). It is therefore of interest to determine how these models perform compared to more rigorous approaches and how these models can be used for extrapolation purposes (Temel et al., 2007). A comparison with our model proposed earlier (Hansen et al., 2009) also offers the opportunity to assess the physical significance of the model parameters in the PL and LH expressions because all the relevant kinetic data is known exactly.

A drawback of the gas phase alkylation of benzene with ethene is the high energy requirement for the production of ethene. One alternative is to use benzene alkylation for reactive separation of ethene derived from another process, e.g. oxidative coupling of methane (Graf and Lefferts, 2009). Another alternative is to use ethane instead of ethene in the feed, i.e. dehydroalkylation. This reaction route requires a dehydrogenation function in the catalyst in addition to the acidic site for alkylation. Benzene alkylation with ethane and propane has been investigated experimentally

* Corresponding authors.
E-mail addresses: n.hansen@tu-harburg.de (N. Hansen), bell@cchem.berkeley.edu (A.T. Bell).

0009-2509/$ - see front matter © 2009 Elsevier Ltd. All rights reserved.
doi:10.1016/j.ces.2009.12.028

over Pt- and Ga-containing zeolites (Ivanova et al., 1996; Derouane et al., 2000; Smirnov et al., 2000, 2001; Kato et al., 2001; Bigey and Su, 2004; Todorova and Su, 2004). However, selectivities towards ethylbenzene and propylbenzene, respectively, were all relatively low due to side reactions such as cracking, oligomerization and isomerization. In a recent study reported by Lukyanov and Vazhnova (2008a, b), benzene alkylation with ethane over Pt-MFI was investigated with the aim to identify reaction conditions and catalysts which provide higher selectivities. It was demonstrated that up to benzene conversion of 10% highly selective and stable benzene alkylation with ethane can be achieved.

In order to simulate this reaction we have extended our reaction–diffusion model (Hansen et al., 2009) to include the dehydrogenation of ethane in addition to the alkylation of benzene. For a theoretical analysis of the dehydrogenation it is essential to know the structure of the active site in order to calculate rate constants for the elementary steps. While in the study of Lukyanov and Vazhnova (2008a, b) Pt was present as nanoparticles on the exterior surface of the zeolite, it has been demonstrated experimentally that Pt can also be dispersed inside the zeolite pore system, either in pure form or as bimetallic species with Ga (Zholobenko et al., 1994; Stakheev et al., 1997; Shpiro et al., 1994a, b; Meriaudeau et al., 1993; Santhosh Kumar et al., 2009). The latter option seems to be more stable (Meriaudeau et al., 1993). In the present work the dehydrogenation activity of small Ga_xPt_y extra-framework particles was studied using density functional theory and rate coefficients of all elementary steps were obtained from absolute rate theory. Using these kinetic data we then extended our diffusion–reaction model for MFI crystals (Hansen et al., 2009) by incorporating the dehydrogenation of ethane in addition to the alkylation of benzene. Diffusivities and adsorption isotherms are obtained from molecular dynamics and Monte Carlo simulations, respectively. This model is then used to simulate the behavior of an isothermal fixed bed reactor. Furthermore, the benefits of using a membrane reactor for this reaction are analyzed.

This paper is organized as follows. Section 2 presents the reactor model and the approach to solve the resulting equations. In Section 3 the performance of LH and PL rate expressions is evaluated against the diffusion–reaction model for the alkylation of benzene with ethene presented earlier (Hansen et al., 2009). Section 4 presents the extension of our reaction–diffusion model by the dehydrogenation of ethane. The methods used to determine the parameters involved in describing adsorption, diffusion, and reactions are presented in Section 5. Section 6 presents simulation results for the alkylation of benzene by ethane and comparison to literature data. The conclusions of this work are presented in Section 7. Details of the simulation methods used to obtain information on the adsorption and diffusion of all species are provided in the Supplementary Material accompanying this article.

2. Reactor model

An isothermal fixed-bed, plug flow reactor is considered for the present study. It is assumed that the intra-crystalline diffusion resistance is the controlling transport phenomenon. Mass transport resistances from the bulk fluid to the catalyst surface as well as diffusion inside the meso- and macropores of the catalyst are neglected. The mole balance for component i in the reactor can be expressed as

$$\frac{dF_i}{dz}+\frac{\tau}{L}\dot{m}\frac{1}{\rho}\frac{3}{R}n_i(z)=0 \tag{1}$$

where F_i is the molar flow rate of species i and z is the length coordinate. The contact time is denoted as τ, L is the length of the reactor, and $\dot{m}$ the mass flow rate through the reactor. The framework density of the MFI crystals is denoted as ρ and the crystal radius as R. The flux of species i at the crystallite outer surface is defined as $n_i(z)$. This flux is calculated from

$$n_i(z)=r_{eff,i}(z)\rho\frac{R}{3} \tag{2}$$

where $r_{eff,i}(z)$ is the effective rate producing or consuming component i inside the catalyst particle, using the reaction–diffusion model we reported earlier (Hansen et al., 2009). This model requires the solution of the partial differential equation describing reaction and diffusion in a spherical geometry. The differential Eq. (1) was solved with Euler's method.

3. Performance of PL and LH models

For the alkylation of benzene both power law (PL) and Langmuir–Hinshelwood (LH) type rate expressions have been used to describe the rate of reaction as function of the process conditions (Smirniotis and Ruckenstein, 1995; Lu et al., 2001; Shi et al., 2001; You et al., 2006). The PL rate expression is given by

$$r_B=\hat{k}_1 p_E^{n_E} p_B^{n_B}-\hat{k}_{-1}p_{EB}^{n_{EB}}, \tag{3}$$

where $\hat{k}_1$ and $\hat{k}_{-1}$ are the apparent rate constants for the forward and reverse reaction, respectively. The partial pressure of component X is denoted as p_X while n_X is the reaction order with respect to component X. The mathematical form of the LH expression depends on the underlying reaction mechanism. If all species are adsorbed and the surface reaction is assumed to be the rate controlling step the LH model reads

$$r_B=\frac{\hat{k}_1 p_B p_E-\hat{k}_{-1}p_{EB}}{(1+K_B p_B+K_E p_E+K_{EB}p_{EB})^2}, \tag{4}$$

We can now take the view that our reaction–diffusion approach with a combination of molecular simulation techniques (Hansen et al., 2009) produces "experimental data" which can be used to obtain the parameters in Eqs. (3) and (4). To find the parameters appearing in the PL and LH models, we have minimized the sum of squares (Gill and Murray, 1978)

$$\min S=\sum_{i=1}^{n}[r_{B,i}(EM)-r_{B,i}(FM)]^2 \tag{5}$$

where $r(EM)$ and $r(FM)$ are the rates obtained using the empirical rate law and the full continuum model, respectively. These rates are determined from fixed bed differential reactor simulations by evaluating

$$r_B=\frac{F_{in}y_{B,in}-F_{out}y_{B,out}}{m_{cat}} \tag{6}$$

where F_{in} and F_{out} are the molar fluxes at the reactor inlet and outlet, respectively, and $y_{B,in}$ and $y_{B,out}$ are the inlet and outlet mole fractions of benzene. The catalyst mass is denoted as m_{cat}. The conversion was always below 2.2% in the differential reactor simulations. For the partial pressures appearing in the PL and LH expressions the arithmetic mean values from the reactor simulations were used.

Sets of 45 rates of reaction were generated at 603 and 653 K by varying the total pressure from 1×10^5 Pa to 5×10^5 Pa and by using 9 subsets of composition at each pressure point. The compositions were chosen such that the benzene to ethene ratio was between 1 and 90 (see Tables SE1 and SE2 in Appendix E for

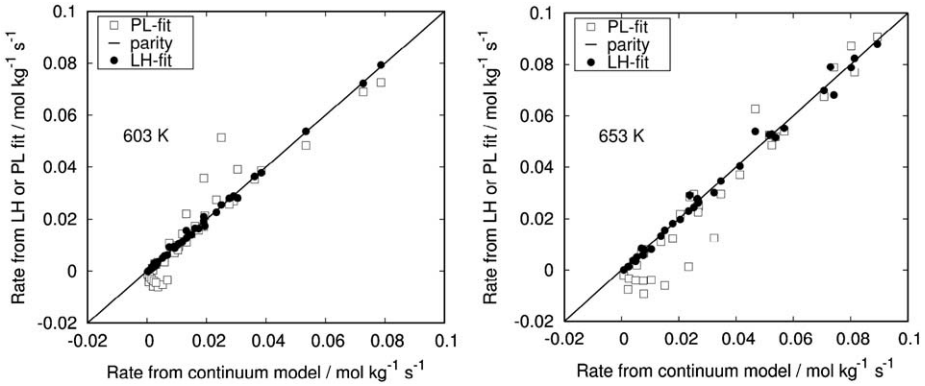

Fig. 1. Comparison of fitted PL and LH rates to those calculated using the full continuum model (Hansen et al., 2009) with intrinsic rate constants of $k_{1603\,K}=1.14\times10^{2}\,s^{-1}$, $k_{-1603\,K}=5.32\times10^{-3}\,s^{-1}$, $k_{1653\,K}=6.96\times10^{2}\,s^{-1}$, and $k_{-1653\,K}=1.37\times10^{-1}\,s^{-1}$.

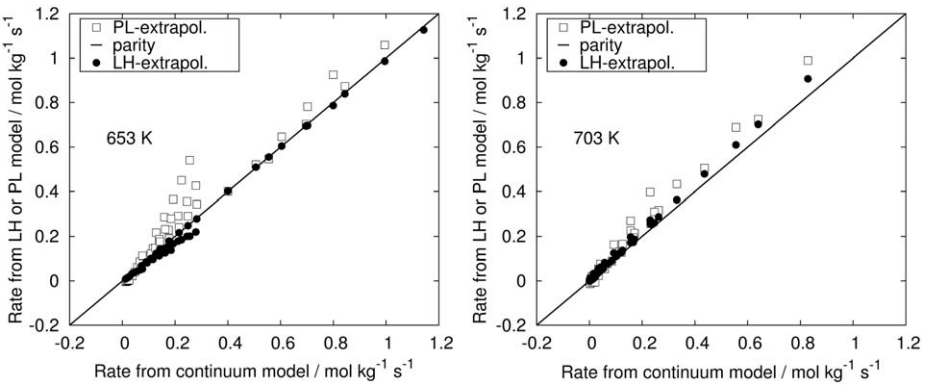

Fig. 2. Comparison of extrapolated PL and LH rates and those of the full model. Left: extrapolation to higher pressures. Right: extrapolation to 703 K at otherwise unchanged pressures and gas phase composition. The intrinsic rate constants used in the full model are $k_{1703\,K}=3.27\times10^{3}\,s^{-1}$ and $k_{-1703\,K}=2.21\times10^{0}\,s^{-1}$.

details). Note that no diffusion limitation was present. The intrinsic rate constants were identical to those used in our previous work (Hansen et al., 2009). The number of acid sites per unit cell was set to 1.1, a value which was also used by us before (Hansen et al., 2009). At both temperatures the data sets could be fitted successfully to the LH expression. The fit to the PL expression was less successful (see Fig. 1) The fit parameters are listed in Tables SE3 and SE4 of the Appendix. Also compiled are the activation energies and pre-exponential factors which were obtained assuming Arrhenius type temperature dependence of all rate and equilibrium constants.

The parity plots shown in Fig. 2 illustrate the extrapolation behavior of both the PL and LH model. For Fig. 2a, a pressure range of 6×10^{5} Pa to 10×10^{5} Pa was used at otherwise unchanged compositions of the feed while for Fig 2b the temperature was changed to 703 K at otherwise unchanged pressures and compositions of the feed. As can be seen from Fig. 2a the rates obtained by extrapolation using the LH expression agree reasonable well with those obtained from the full continuum model. At some points the simulated rates are slightly underestimated. By contrast the rates predicted by the PL model overestimate those of the full continuum model. When extrapolating to higher temperatures, both the PL and LH model over-predict the rates of the full continuum model. It should be noted though that in order to extrapolate with the PL model, the parameters had to be fitted to 603 and 653 K simultaneously with fixed values for the exponents, which reduces the numbers of adjustable parameters compared to the LH model. As can be seen from the individual fits (Table SE4), the exponent for benzene in the PL expression depends strongly on the temperature and consequently large uncertainties are introduced into this model when using it to fit rate data over a broad temperature range. The activation energy parameter was extracted from the values of k at 603 and 653 K. For the LH model a value of $E_1=44.3$ kJ/mol is obtained while the PL model gives $E_1=68.0$ kJ/mol. The apparent activation energies calculated with the full continuum model are strongly dependent on both the total pressure and the gas phase composition. At 1×10^{5} Pa apparent activation energies are in the range from 49 to 60 kJ/mol while at 5×10^{5} Pa E_a ranges from 66 to 90 kJ/mol (gas phase mole fractions of C_6H_6, C_2H_4, C_8H_{10}: 0.50, 0.49, 0.01 and 0.50, 0.25, 0.25). From these results it is obvious that the LH and PL models do not offer the required flexibility to calculate the rates for the alkylation of benzene with ethene over a wide range of process conditions. Due to the strong dependence of the apparent activation energies on total pressure and gas phase composition an unambiguous interpretation of the energy parameters appearing in the LH and PL expression as activation energies is not possible. It is now of interest to determine how the LH and PL models perform when using them in a reactor design equation. This is illustrated in Figs. 3 and 4. The conversions in Fig. 3 have been determined for a benzene to ethene ratio in the feed of 5:1. As a consequence the molar fractions of all species were within or close to the fitting range. The conversion calculated with the LH expression are in reasonably good agreement with the full continuum model while the PL model overestimates the conversion for low contact times and underestimates the maximum conversion. At 703 K, both the LH and the PL model are in good agreement with the continuum simulations up to a contact time of 0.003 h. For larger contact times the PL model underestimates the simulation while the LH

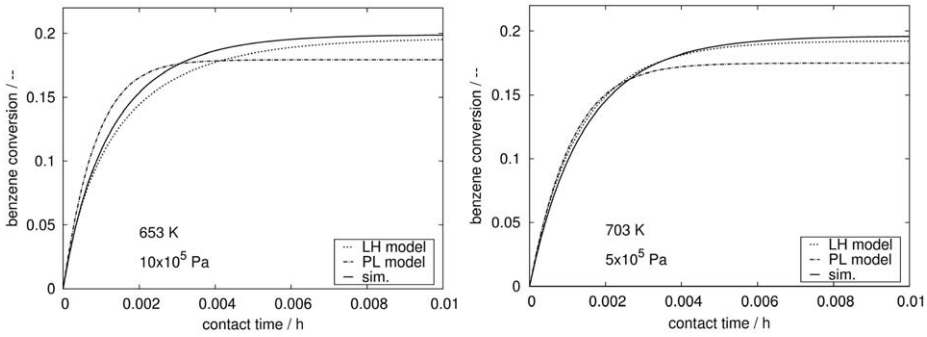

Fig. 3. Effect of contact time on the conversion of benzene at 653 and 703 K for a benzene to ethene molar ratio in the feed of 5:1.

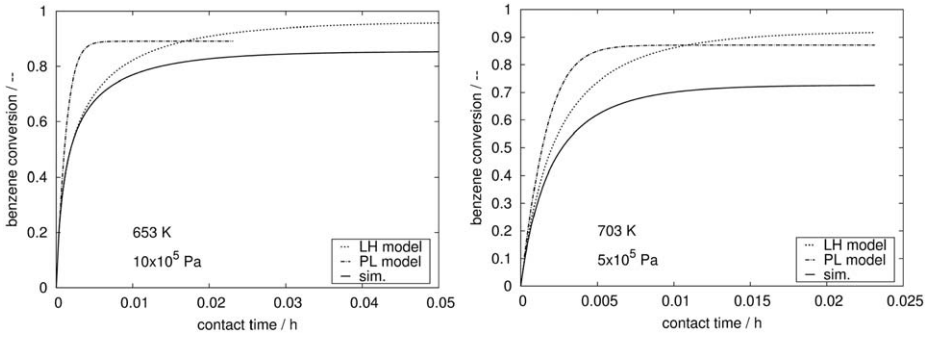

Fig. 4. Effect of contact time on the conversion of benzene at 653 and 703 K for a benzene to ethene molar ratio in the feed of 2:3.

model is in good agreement with the continuum simulations up to the maximum conversion.

In calculating the simulation results shown in Fig. 4 the composition of the feed gas was changed to a benzene/ethene ratio of 2/3. As can be seen, both LH and PL models deviate significantly from the continuum simulations. Interestingly the maximum conversion predicted by our model is below the gas phase equilibrium conversion which is close to unity. This is a consequence of the strong adsorption of the product (ethylbenzene) which leads to a shift in the equilibrium composition towards the reactant side. This behavior is also captured qualitatively by the LH and the PL model. However, both models predict significantly higher equilibrium conversions than the full continuum simulations. The degree to which the maximum conversion predicted by the continuum model stays below the gas phase equilibrium conversion depends on the ratio of intrinsic rate coefficients as predicted by the quantum chemical method as well as on the adsorption properties of ethylbenzene calculated using the ideal adsorbed solution theory which draws upon adsorption isotherms obtained from Monte Carlo simulations in the grand canonical ensemble (Hansen et al., 2009). Experimental evidence for this behavior is rare. However, a maximum in transient kinetic data for the alkylation of benzene over zeolite Y could be explained by a build-up of ethylbenzene in the zeolite due to a strong adsorption constant (Nolley and Katzer, 1973).

The present results support earlier studies that have shown the importance of a correct description of multicomponent adsorption by the ideal adsorbed solution theory instead of the multicomponent Langmuir description underlying the conventional LH rate expression (Krishna and Baur, 2005; Baur and Krishna, 2005). In what follows we concentrate on our continuum model and extend it to the ethane dehydrogenation reaction. The replacement of ethene by ethane as the alkylating agent using a bifunctional catalyst is an economically attractive option because alkanes are major constituents of natural gas and therefore widely available (Labinger and Bercaw, 2002).

4. Dehydrogenation of ethane

The dehydrogenation of ethane to ethene and hydrogen is a strongly equilibrium limited endothermic reaction. The mechanism of this reaction carried out over Ga_xPt_y-species comprises a series of steps all of which show small activation energies (see Appendix D). The theoretically determined rate coefficients for the dehydrogenation are larger than those for the alkylation over acid sites. This has two consequences. First, it is not necessary to consider all elementary steps leading to ethene and hydrogen in the model because the formation of ethene is a rapid process compared to the formation of ethylbenzene. This allows us to describe the intrinsic rate of reaction as following a one-step scheme with effective values for the forward and reverse rate coefficient:

$$r_{deh} = k_1 q_{C2} - k_{-1} q_E q_H, \tag{7}$$

where k_1 and k_{-1} are the intrinsic rate coefficients for the forward and reverse reaction, respectively and q_i denotes the loading of species i inside the zeolite channels. Second, it is necessary to ensure that the correct chemical equilibrium composition is approached inside the zeolite pores. Therefore we express the net forward reaction rate as

$$r_{deh} = k_1 \alpha \left(q_{C2} - \frac{1}{K_q} q_E q_H \right), \tag{8}$$

which avoids the problem of finding a rate coefficient for the reverse reaction. The value of k_1 is derived from quantum chemical calculations as described in Appendix D. The factor α

should account for the fact that only a fraction of the ethane is available for the dehydrogenation. It can be interpreted as the conditional probability that an ethane molecule which is adsorbed inside the zeolite pores is located close enough to a dehydrogenation site to be converted. As will be shown below, the simulation results are essentially independent of α which makes a detailed model unnecessary. The equilibrium constant K_q is defined as

$$K_q = \frac{q_H^{eq} q_E^{eq}}{q_{C2}^{eq}} \tag{9}$$

where q_X^{eq} is the loading of component X at chemical equilibrium. It should be emphasized that the mole fractions of the adsorbates in chemical equilibrium are not equal to the equilibrium mole fractions in the gas phase due to differences in the adsorption strength of the different species (Hansen et al., 2005; Jakobtorweihen et al., 2006; Turner et al., 2008). This leads to a shift in the chemical equilibrium in the adsorbed phase towards the reactant side. In the case of thermodynamic equilibrium we can couple the equilibrium constant appearing in Eq. (9) to the gas phase equilibrium constant K_a calculated from the Gibbs free energy of reaction. When using the ideal adsorbed solution theory (Myers and Prausnitz, 1965) for the calculation of the adsorbed amounts, thermodynamic equilibrium is expressed as

$$p_i^0 x_i = p y_i \tag{10}$$

where x and y represent the mole fractions in the adsorbed and gas phase, respectively. The total pressure in the gas phase is denoted as p, while p_i^0 is the pressure of component i in the gas phase in equilibrium with an amount adsorbed that exerts the same spreading pressure of the mixture. With these quantities we are then able to express the equilibrium constant in terms of activities, K_a, by

$$\begin{aligned} K_a &= \prod_i a_i^{\nu_i} = (10^5\ \mathrm{Pa})^{-\sum \nu_i} K_P = (10^5\ \mathrm{Pa})^{-\sum \nu_i} \frac{p_H^{eq} p_E^{eq}}{p_{C2}^{eq}} \\ &= (10^5\ \mathrm{Pa})^{-\sum \nu_i} \frac{x_H^{eq} p_H^o x_E^{eq} p_E^o}{x_{C2}^{eq} p_{C2}^o} = (10^5\ \mathrm{Pa})^{-\sum \nu_i} \frac{q_H^{eq} p_H^o q_E^{eq} p_E^o}{q_{tot}^{eq} q_{C2}^{eq} p_{C2}^o} \end{aligned} \tag{11}$$

The latter expression can then be rearranged to give a relation between the gas phase equilibrium constant, K_a, and the one calculated from the equilibrium adsorbed amounts.

$$K_q = \frac{q_H^{eq} q_E^{eq}}{q_{C2}^{eq}} = K_a (10^5\ \mathrm{Pa}) q_{tot}^{eq} \frac{p_{C2}^o}{p_H^o p_E^o} \tag{12}$$

For reactor simulations of the dehydroalkylation Eq. (1) has to be integrated subject to the constraint imposed by the chemical equilibrium of the dehydrogenation reaction. Therefore we have used an adaptive step size control which guarantees that

$$\frac{y_H(z) y_E(z)}{y_{C2}(z)} \le \frac{K_a}{\dfrac{p}{10^5\ \mathrm{Pa}}} \tag{13}$$

along the length coordinate z.

5. Parameterization

Pure component adsorption isotherms for ethane and hydrogen were obtained by MC simulations using the method described in Appendix A of the Supporting Information. These isotherms were fitted to analytical isotherm models (see Appendix B of the Supporting Information). Adsorption isotherms for ethene, benzene, and ethylbenzene were taken from our previous work (Hansen et al., 2009). Mixture adsorption isotherms were then calculated from the pure component adsorption isotherms by means of the IAST. Multicomponent diffusion was characterized by means of the Maxwell–Stefan equations (Krishna, 2009). The diffusivity data for ethene, benzene, and ethylbenzene were taken from our previous work (Hansen et al., 2009). The Maxwell–Stefan (M–S) diffusivities of ethane and hydrogen were obtained from MD calculations (see Appendix C). In our previous work we have adapted the magnitude of the diffusivities by fitting them to experimental results from diffusion-limited rate data. This became necessary because of the limited reliability of results from conventional MD simulations for diffusion of aromatic hydrocarbons in zeolites (see Hansen et al. (2009) for details). The final M–S diffusivities for benzene and ethylbenzene were then of the order of $10^{-13}\ \mathrm{m^2\,s^{-1}}$ at reaction temperature which is still in agreement with experimental data (Masuda et al., 1998; Nakasaka et al., 2008). To be consistent with our earlier publication (Hansen et al., 2009) we have scaled down the zero-loading M–S diffusivities of ethane and hydrogen by 3.4 orders of magnitude. The unscaled diffusivities of ethane and hydrogen are listed in Table SC1 in Appendix C. The rate coefficients for the dehydrogenation of ethane were determined from quantum chemical calculation as outlined in Appendix D of the Supporting Information. The rate coefficients for the alkylation reaction were determined in two steps. Initially the rate coefficients determined in our previous study (Hansen et al., 2009) were taken to simulate the effect of contact time on the conversion of benzene and the results were compared to the experimental data reported by Lukyanov and Vazhnova (2008b). These data were measured for a zeolite sample with a Si/Al ratio of 15 which corresponds to six acid sites per unit cell provided that every negative charge introduced by an Al is compensated by a proton. The size of the crystallites was reported to be in the range from 0.4 to 0.7 μm. As a result diffusion limitation is unlikely to occur. In our simulations we have used a value of 6 acid sites per unit cell. The number of dehydrogenation sites is proportional to the factor α in Eq. (8). However, for α being in the range from 0.01 to 1 essentially no change in the dehydroalkylation activity is observed because the dehydrogenation reaction is significantly faster than the alkylation. It turned out, however, that the experimental alkylation activity was underestimated. Therefore we increased the rate coefficient for the alkylation by a factor of four, a value which is acceptable when attempting quantitative predictions from first principles. We have also decided to increase the simulation

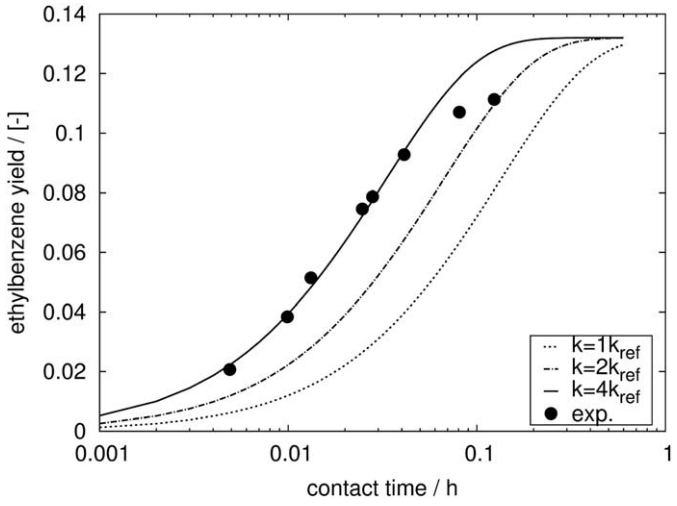

Fig. 5. Adjustment of rate coefficients to experimental data. The experimental data are reported for a total pressure of 1×10^5 Pa and ethane to benzene molar ratio in the feed of 9:1. The conditions for the simulations were $p = 2 \times 10^5$ Pa, $y_B = 0.1$, $y_{C2} = 0.9$, and $k_{ref} = 6.96 \times 10^2\ \mathrm{s^{-1}}$.

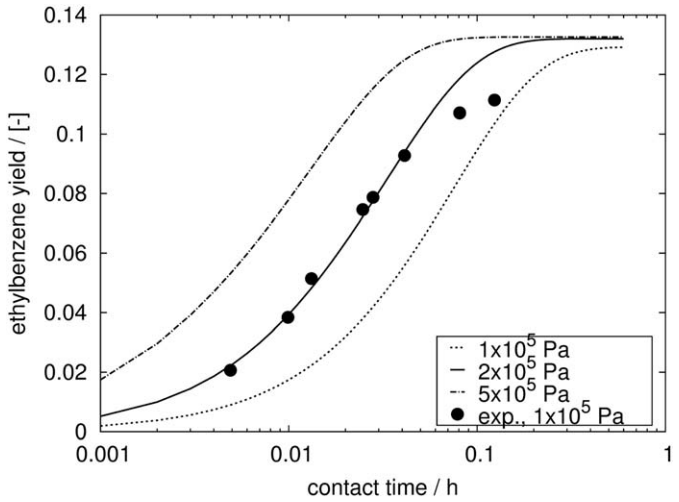

Fig. 6. Effect of contact time and pressure on benzene conversion at 653 K for an ethane to benzene molar ratio in the feed of 9:1.

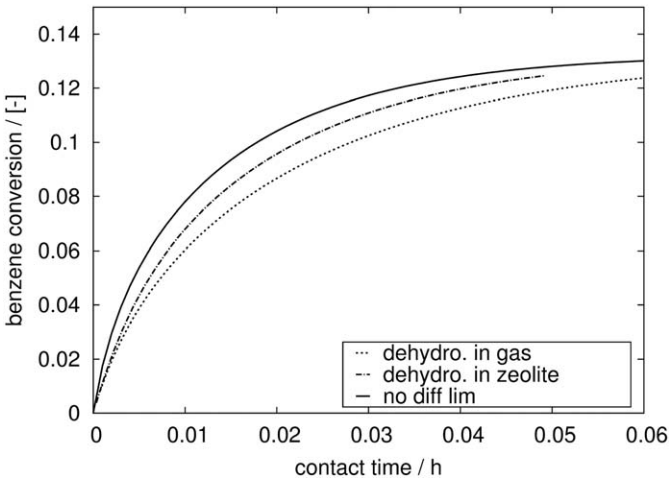

Fig. 7. Effect of diffusion limitation on the benzene conversion at 653 K and 5×10^5 Pa for an ethane to benzene molar ratio in the feed of 9:1 and a particle size of 2 μm. The full line represents the conversion without diffusion limitation. The dotted and the dot and dash line represent dehydrogenation in the gas phase and the zeolite, respectively.

Table 1
Equilibrium constant for ethane dehydrogenation and intrinsic rate coefficients at 653 K.

Reaction	Constant	
$C_2H_6 \leftrightarrow C_2H_4 + H_2$	k_1, s^{-1}	5.00E+03
	K_a, –	4.21E−05
$C_6H_6 + C_2H_4 \leftrightarrow C_8H_{10}$	k_1, s^{-1}	2.78E+03
	k_{-1}, s^{-1}	5.480E−01

pressure from 1×10^5 Pa to 2×10^5 Pa in order to match the experimental curve. The influence of the intrinsic rate coefficient and the total pressure on the simulated conversion-over-contact time-plots is illustrated in Figs. 5 and 6. The fitting strategy is similar to our earlier work (Hansen et al., 2009) and tries to take into account both, errors in the adsorption isotherms as well as errors in the quantum chemical approaches used to determine the rate coefficients. The resulting rate coefficients are listed in Table 1. In Fig. 5 we have plotted the ethylbenzene yield instead of the benzene conversion because of the occurrence of side reactions for higher contact times. These side reactions are responsible for a benzene conversion higher than the equilibrium conversion in the experiments reported by Lukyanov and Vazhnova (2008b). For the simulations ethylbenzene yield and benzene conversion are identical as no side reactions are considered.

6. Results and discussion

6.1. Intrinsic kinetics

The intrinsic kinetics can be established by using the rates of reaction on the crystal surface. The solution of the diffusion–reaction equation is not necessary because the rates depend solely on the adsorbed amounts. Fig. 6 shows the effects of the input pressure on the contact time needed to get the maximum conversion for a ethane–benzene mixture of 9:1. As expected the increase of the inlet pressure leads to a decrease of the contact time and thus the amount of catalyst needed to reach full conversion. The maximum conversion predicted by the model stays slightly below the gas phase equilibrium conversion (14.5%). The reason is that with increasing conversion the concentration of adsorbed ethylbenzene increases and, consequently, the rate of the reverse reaction. As stated above, the degree to which the gas phase equilibrium is underestimated depends on the accuracy to which the ratio of rate coefficients was calculated by the quantum mechanical method and the accuracy of the adsorption isotherms obtained from Monte Carlo simulations. The finding that the maximum conversion predicted by the continuum model does not exceed the gas phase equilibrium conversion shows that the parameters describing adsorption and intrinsic reactions are consistent while it does not provide a quantitative prediction for the equilibrium conversion.

6.2. Effects of diffusion limitation

The effect of diffusion limitation on the dehydroalkylation activity was studied for two different scenarios. In the first scenario it is assumed that the dehydrogenation of ethane takes place in the gas phase while in the second scenario the dehydrogenation occurs inside the zeolite. The first scenario corresponds to the experimental situation in which the dehydrogenation function is located on the outer particle surface (e.g. as nanoparticles) while the second scenario corresponds to the picture of dispersed dehydrogenation sites inside the zeolite channels. Simulations have been conducted for a catalyst particle size of 2 μm at 5×10^5 Pa gas phase pressure. Fig. 7 shows that the contact time required to achieve a certain conversion increases in the case of diffusion limitation, as expected. More interestingly it can be observed that the catalyst activity is higher when the dehydrogenation occurs inside the pores compared to the dehydrogenation in the gas phase. When ethene is produced exclusively in the gas phase it has to diffuse into the zeolite pores in order to be converted. The ethene production inside the pores has the advantage that the concentration profile of ethene inside the catalyst particle is less depleted and, consequently, the ethene concentration in the particle center is higher which leads to a higher rate of reaction. Both situations are illustrated in Fig. 8 which presents the ethene occupancy profiles, $\theta_E(\xi) = q_E(\xi)/q_{E,sat}$, over the radial coordinate ξ for both scenarios at a position close to the reactor inlet. This example nicely illustrates the potential of the simulation approach to gain insight into complex reaction systems.

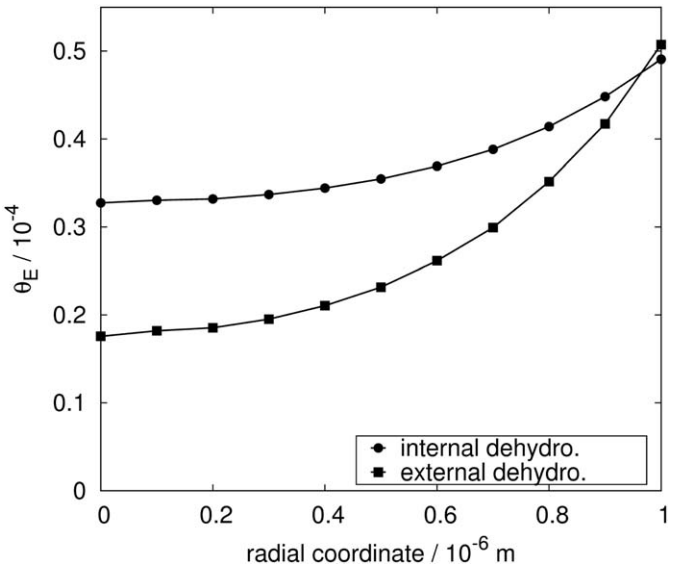

Fig. 8. Radial occupancy profiles of ethene close to the reactor inlet for external and internal dehydrogenation at 653 K and 5×10^5 Pa for an ethane to benzene molar ratio in the feed of 9:1 and a particle size of 2 μm.

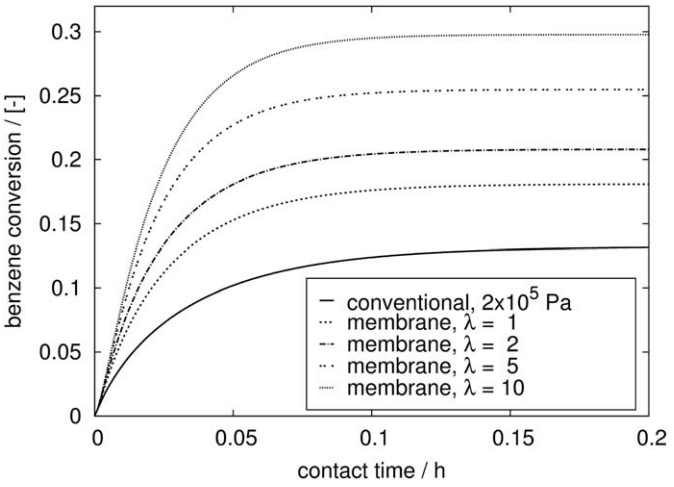

Fig. 9. Effect of hydrogen removal on benzene conversion at 653 K and 2×10^5 Pa for an ethane to benzene molar ratio in the feed of 9:1. The pressure in the permeate stream was fixed to 1×10^5 Pa.

6.3. *Effects of hydrogen removal*

Dehydroalkylation is strongly limited by thermodynamic equilibrium. An attractive approach is the use of a membrane reactor with a hydrogen selective membrane. Beside the increase in benzene conversion this process would offer the benefit of separating the high valuable hydrogen from the reaction mixture (Rezai and Traa, 2008). Here we have simulated a membrane reactor assuming hydrogen pressure equilibrium across the membrane, that is, after each integration step the hydrogen partial pressures on retentate and permeate sides were equilibrated by allowing hydrogen to flow from the reaction zone into the permeate stream. Fig. 9 shows the effects of the ratio λ between sweep gas flow and reactant feed on the equilibrium conversion of benzene. It can be seen that the benzene conversion can be increased significantly by removing hydrogen from the reaction zone. For the highest simulated ratio (λ=10) the benzene conversion is 30% which is an almost threefold increase compared to the normal fixed bed operation mode.

7. Conclusions

One of the key challenges in reaction engineering is the development of improved science-based scale-up methodologies leading to more efficient processes (Dudukovic, 2010). This can be accomplished by a multiscale approach combining atomistic and continuum modelling. In the present work we have performed reactor simulations for the alkylation of benzene with ethene in zeolite H-ZSM-5 based on a detailed continuum description of the reaction system. Kinetic data generated in the differential operation mode of the reactor were used to parameterize Langmuir–Hinshelwood and power-law rate expressions. These rate expressions were then used to extrapolate to higher pressure and temperature and in a design equation for a fixed bed reactor. It was demonstrated that the LH rate expression shows extrapolation capabilities comparable to the predictions of the continuum model as long as the gas phase composition remains within the fitting range. By contrast, the predictions of the power law rate expression deviate from those of the LH rate expression and the continuum model. In particular, a lower maximum conversion achievable in a fixed bed reactor was predicted. When the gas phase composition deviates significantly from that used for fitting, both the LH and the PL rate expressions deviate considerably from the predictions of the full continuum model and predict a higher maximum conversion in fixed bed reactor simulations. These results suggest that for zeolite-catalyzed reactions producing strongly adsorbed products such as ethylbenzene LH and PL rate expressions may lack the required flexibility to describe the limit of full conversion.

The second objective of the present work was to include the dehydrogenation of ethane into our continuum model. The rate coefficients for this reaction were estimated by means of density functional calculations and absolute rate theory. The full model was shown to predict correctly the behavior of a fixed bed reactor for the dehydroalkylation. Moreover, we have demonstrated the potential of a membrane reactor for this reaction. The removal of hydrogen from the reactant mixture can increase the benzene conversion significantly.

All of these applications illustrate how detailed atomistic simulations can be linked to macroscopic reactor models in order to achieve a superior predictability compared to empirical kinetic rate expressions.

Notation

Latin letters

a_i	activity of species *i*, dimensionless
F_i	molar flow rate of species *i*, mol s^{-1}
k	intrinsic reaction rate coefficient, s^{-1}
K	adsorption equilibrium constant, Pa^{-1}
K_a	chemical equilibrium constant, dimensionless
K_q	reaction equilibrium constant in adsorbed phase, mol kg^{-1}
$\hat{k}$	apparent reaction rate coefficient, mol kg^{-1} s^{-1} Pa^{-n}
L	length of reactor, m
m_{cat}	catalyst mass, kg
$\dot{m}$	mass flow rate, kg s^{-1}
n	molar flow through outer surface, mol s^{-1} m^{-2}

n exponent in power law, dimensionless
p pressure, Pa
q_i molar loading of species i, mol kg^{-1}
r rate of reaction, mol kg^{-1} s^{-1}
R radius of crystalline catalyst, m
x_i adsorbed phase mole fraction of species i, dimensionless
y_i gas phase mole fraction of species i, dimensionless
z length coordinate, m

Greek letters

α factor accounting for number of dehydrogenation sites, dimensionless
θ_i fractional occupancy of component i, dimensionless
λ ratio between sweep gas flow and reactant feed, dimensionless
ν_i stoichiometric coefficient of species i, dimensionless
ξ diffusion path, m
ρ framework density of zeolite, kg m^{-3}
τ contact time ($m_{cat}/\dot{m}$), s

Subscripts

B benzene
C2 ethane
eff effective
E ethene
EB ethylbenzene
H hydrogen
sat referring to saturation conditions

Superscripts

eq referring to chemical equilibrium

Acknowledgments

The present work was supported by the Deutsche Forschungsgemeinschaft (DFG) in priority program SPP 1155 and the Methane Conversion Cooperative supported by BP.

Appendix A. Supplementary material

Supplementary data associated with this article can be found in the online version at doi:10.1016/j.ces.2009.12.028.

References

Baur, R., Krishna, R., 2005. The effectiveness factor for zeolite catalysed reactions. Catalysis Today 105, 173–179.
Berger, R.J., Stitt, E.H., Marin, G.B., Kapteijn, F., Moulijn, J.A., 2001. Chemical reaction kinetics in practice. CATTECH 5, 30–60.
Bigey, C., Su, B.-L., 2004. Propane as alkylating agent for alkylation of benzene on HZSM-5 and Ga-modified HZSM-5 zeolites. Journal of Molecular Catalysis A: Chemical 209, 179–187.
Bos, A.N.R., Lefferts, L., Marin, G.B., Steijns, M.H.G.M., 1997. Kinetic research on heterogeneously catalysed processes: a questionnaire on the state-of-the-art in industry. Applied Catalysis A: General 160, 185–190.
Derouane, E.G., He, H., Derouane-Abd Hamid, S.B., Lambert, D., Ivanova, I.I., 2000. In situ MAS NMR spectroscopy study of catalytic reaction mechanisms. Journal of Molecular Catalysis A: Chemical 158, 5–17.
Dudukovic, M.P., 2010. Reaction engineering: Status and future challenges. Chemical Engineering Science 65, 3–11.
Dwyer, F.G., Lewis, P.J., Schneider, F.H., 1976. Efficient, non-polluting ethylbenzene process. Chemical Engineering 83, 90–91.
Gill, P.E., Murray, W., 1978. Algorithms for the solution of the nonlinear least-squares problem. SIAM Journal on Numerical Analysis 15, 977–992 NAG-routine E04FYF.
Graf, P.O., Lefferts, L., 2009. Reactive separation of ethylene from the effluent gas of methane oxidative coupling via alkylation of benzene to ethylbenzene on ZSM-5. Chemical Engineering Science 64, 2773–2780.
Haag, W.O., Olson, D.H., Weisz, P.B., Shape-selective catalysis in aromatics processing. In: Grünwald, H., (Ed.), Chemistry for the Future, Proceedings of the 29th IUPAC Congress, Pergamon Press, Oxford, p. 327.
Hansen, N., Jakobtorweihen, S., Keil, F.J., 2005. Reactive Monte Carlo and grand-canonical Monte Carlo simulations of the propene metathesis reaction system. The Journal of Chemical Physics 122 164705-1/11.
Hansen, N., Brüggemann, T., Bell, A.T., Keil, F.J., 2008. Theoretical investigation of benzene alkylation with ethene over H-ZSM-5. Journal of Physical Chemistry C 112, 15402–15411.
Hansen, N., Krishna, R., van Baten, J.M., Bell, A.T., Keil, F.J., 2009. Analysis of diffusion limitation in the alkylation of benzene with ethene over H-ZSM-5 by combining quantum chemical calculations, molecular simulations, and a continuum approach. Journal of Physical Chemistry C 113, 235–246.
Ivanova, I.I., Blom, N., Derouane, E.G., 1996. C MAS NMR mechanistic study of benzene alkylation with propane over Ga-modified H-ZSM-5 catalyst. Journal of Molecular Catalysis A: Chemical 109, 157–168.
Jakobtorweihen, S., Hansen, N., Keil, F.J., 2006. Combining reactive and configurational-bias Monte Carlo: Confinement influence on the propene metathesis reaction system in various zeolites. The Journal of Chemical Physics 125 224709–1/9.
Kato, S., Nakagawa, K., Ikenaga, N., Suzuki, T., 2001. Alkylation of benzene with ethane over platinum loaded zeolite catalyst. Catalysis Letters 73, 175–180.
Krishna, R., Baur, R., 2005. On the Langmuir–Hinshelwood formulation for zeolite catalysed reactions. Chemical Engineering Science 60, 1155–1166.
Krishna, R., 2009. Describing the diffusion of guest molecules inside porous structures. Journal of Physical Chemistry C 113, 19756–19781.
Labinger, J.A., Bercaw, J.E., 2002. Understanding and exploiting C–H bond activation. Nature 417, 507–514.
Lu, M., Wu, Y., Zhu, Z., Sun, H., Chen, Q., 2001. Ethylbenzene synthesis over AB-97 zeolite. I. The intrinsic kinetics and macrokinetics. Petrochemical Technology (China) 30, 182–187.
Lukyanov, D.B., Vazhnova, T., 2008a. Highly selective and stable alkylation of benzene with ethane into ethylbenzene over bifunctional PtH-MFI catalysts. Journal of Molecular Catalysis A: Chemical 279, 128–132.
Lukyanov, D.B., Vazhnova, T., 2008b. A kinetic study of benzene alkylation with ethane into ethylbenzene over bifunctional PtH-MFI catalyst. Journal of Catalysis 257, 382–389.
Masuda, T., Fujikata, Y., Nishida, T., Hashimoto, K., 1998. The influence of acid sites on intracrystalline diffusivities within MFI-type zeolites. Microporous and Mesoporous Materials 23, 157–167.
Meriaudeau, P., Sapaly, G., Naccache, C., 1993. T.E.M. and catalytic property study of Pt-Ga on HZSM-5. In: Proceedings of the Ninth International Zeolite Conference. Butterworth-Heinemann, Boston, pp. 583–589.
Mezaki, R., Inoue, H. (Eds.), 1991. Rate Equations for Solid-Catalyzed Reactions. University of Tokyo Press, Tokyo.
Myers, A.L., Prausnitz, J.M., 1965. Thermodynamics of mixed gas adsorption. A.I.Ch.E. Journal 11, 121–127.
Nakasaka, Y., Tago, T., Odate, K., Masuda, T., 2008. Measurement of intracrystalline diffusivity of benzene within MFI-type zeolite from bulk benzene/cyclohexane liquid phase. Microporous and Mesoporous Materials 112, 162–169.
Nolley, J.P., Katzer, J.R., 1973. Desorption influence on benzene alkylation with olefins over Y zeolites. Advances in Chemistry 121, 563–574.
Perego, C., Ingallina, P., 2002. Recent advances in the industrial alkylation of aromatics: new catalysts and new processes. Catalysis Today 73, 3–22.
Rezai, S.A.S., Traa, Y., 2008. Equilibrium shift in membrane reactors: a thermodynamic analysis of the dehydrogenative conversion of alkanes. Journal of Membrane Science 319, 279–285.
Santhosh Kumar, M., Holmen, A., Chen, D., 2009. The influence of pore geometry of Pt containing ZSM-5, Beta and SBA-15 catalysts on dehydrogenation of propane. Microporous and Mesoporous Materials 126, 152–158.
Shi, Y., Gao, Y., Dai, Y., Yuan, W., 2001. Kinetics for benzene plus ethylene reaction in near critical regions. Chemical Engineering Science 56, 1403–1410.
Shpiro, E.S., Shevchenko, D.P., Tkachenko, O.P., Dmitriev, R.V., 1994a. Platinum promoting effects in Pt/Ga zeolite catalysts of lower alkane aromatization. I. Ga and Pt electronic states, dispersion and distribution in zeolite crystals in dependence of preparation techniques. Dynamic effects caused by reaction mixture. Applied Catalysis A: General 107, 147–164.
Shpiro, E.S., Shevchenko, D.P., Dmitriev, R.V., Tkachenko, O.P., Minachev, K.M., 1994b. Platinum promoting effects in Pt/Ga zeolite catalysts of lower alkane aromatization. II. The catalytic properties in n-butane aromatization, formation of the catalytically active sites and reaction mechanism. Applied Catalysis A: General 107, 165–180.
Smirniotis, P.G., Ruckenstein, E., 1995. Alkylation of benzene or toluene with MeOH or C_2H_4 over ZSM-5 or beta-zeolite–effect of zeolite pore openings and of the hydrocarbons involved on the mechanism of alkylation. Industrial and Engineering Chemistry Research 34, 1517–1528.
Smirnov, A.V., Mazin, E.V., Yuschenko, V.V., Knyazeva, E.E., Nesterenko, S.N., Ivanova, I.I., Galperin, L., Jensen, R., Bradley, S., 2000. Benzene alkylation with propane over Pt-modified MFI zeolites. Journal of Catalysis 194, 266–277.
Smirnov, A.V., Mazin, E.V., Ponomoreva, O.A., Knyazeva, E.E., Nesterenko, S.N., Ivanova, I.I., 2001. Benzene alkylation with alkanes over modified MFI catalysts. Studies in Surface Science and Catalysis 135, 153.

Stakheev, A.Y., Shpiro, E.S., Tkachenko, O.P., Jaeger, N.I., Schulz-Ekloff, G., 1997. Evidence for monoatomic platinum species in H-ZSM-5 from FTIR spectroscopy of chemisorbed CO. Journal of Catalysis 169, 382–388.

Temel, B., Meskine, H., Reuter, K., Scheffler, M., Metiu, H., 2007. Does phenomenological kinetics provide an adequate description of heterogeneous catalytic reactions. The Journal of Chemical Physics 126 204711-1/12.

Todorova, S., Su., B.-L., 2004. Effects of acidity and combination of Ga and Pt on catalytic behavior of Ga-Pt modified ZSM-5 catalysts in benzene alkylation with pure propane. Catalysis Today 93-95, 417–424.

Turner, C.H., Brennan, J.K., Lísal, M., Smith, W.R., Johnson, J.K., Gubbins, K.E., 2008. Simulation of chemical reaction equilibria by the reaction ensemble Monte Carlo method: a review. Molecular Simulation 34, 119–146.

Weitkamp, J., 1985. Alkylation of hydrocarbons with zeolite catalysts—commercial applications and mechanistic aspects. Acta Physica et Chemica (Szeged) 31, 271–290.

Weitkamp, J., Puppe, L., 1999. Catalysis and Zeolites—Fundamentals and Applications. Springer, Berlin.

You, H., Long, W., Pan, Y., 2006. The Mechanism and kinetics for the alkylation of benzene with ethylene. Petroleum Science and Technology 24, 1079–1088.

Zholobenko, V.L., Lei, G.-D., Carvill, B.T., Lerner, B.A., Sachtler, W.M.H., 1994. Identification of isolated Pt atoms in H-mordenite. Journal of the Chemical Society, Faraday Transactions 90, 233–238.